Physica E: Low-dimensional Systems and Nanostructures 101 (2018) 22–28

Contents lists available at ScienceDirect

Physica E: Low-dimensional Systems and Nanostructures

journal homepage: www.elsevier.com/locate/physe

Self-similar transmission patterns induced by magnetic field effects in graphene

R. Rodríguez-González [a], I. Rodríguez-Vargas [a,*], D.S. Díaz-Guerrero [a], L.M. Gaggero-Sager [b]

[a] Unidad Académica de Física, Universidad Autónoma de Zacatecas, Calzada Solidaridad Esquina con Paseo la Bufa S/N, 98060, Zacatecas, Zac., Mexico
[b] Centro de Investigación en Ingeniería y Ciencias Aplicadas, Universidad Autónoma del Estado de Morelos, Av. Universidad 1001, Col. Chamilpa, 62209, Cuernavaca, Morelos, Mexico

ARTICLE INFO

Keywords:
Self-similarity
Scaling rules
Transmittance
Magnetic field
Cantor structures

ABSTRACT

In this work we study the propagation of Dirac electrons through Cantor-like structures in graphene. In concrete, we are considering structures with magnetic and electrostatic barriers arrange in Cantor-like fashion. The Dirac-like equation and the transfer matrix approach have been used to obtain the transmission properties. We found self-similar patterns in the transmission probability or transmittance once the magnetic field is incorporated. Moreover, these patterns can be connected with other ones at different scales through well-defined scaling rules. In particular, we have found two scaling rules that become a useful tool to describe the self-similarity of our system. The first expression is related to the generation and the second one to the length of the Cantor-like structure. As far as we know it is the first time that a special self-similar structure in conjunction with magnetic field effects give rise to self-similar transmission patterns. It is also important to remark that according to our knowledge it is fundamental to break some symmetry of graphene in order to obtain self-similar transmission properties. In fact, in our case the time-reversal symmetry is broken by the magnetic field effects.

1. Introduction

In nature many peculiar features of certain phenomena are observable only under special conditions. For instance, recently by breaking either the time-reversal symmetry or the inversion symmetry novel materials such as topological insulators [1–3], Dirac semimetals [4,5], Weyl semimetals [6,7] and materials with special charge carriers like Kane electrons [8,9] have arisen. Then, the set of symmetries in a material (chiral symmetries) and specially its breaking (chiral symmetry breaking) can give rise to unprecedented materials with exotic properties. In fact, in graphene it has been shown that chiral symmetry breaking can change the character of the material from a semimetal to a strong insulator [10]. Even a metallic or superconducting phase can be induced by breaking some particular chiral symmetry. Actually, if we take into account the variety of 2D materials available today as well as the symmetry-breaking possibilities the opportunities for exotic materials are superb.

On the other hand, the two-dimensional nature of graphene constitutes an unprecedented platform to study the transmission and transport properties in special (self-similar) geometries such as those that can be constructed using the Sierpinski carpet, Cantor set, Koch curve, etc. In principle, these peculiar geometries can be obtained by nanostructuring the material. In fact, it is possible to obtain potential profiles with self-similar characteristics. Even, the profiles can have scaling in both the spatial and energy axis. These self-similar potential profiles were originally proposed in the context of semiconductor quantum wells [11,12]. Actually, in graphene we have several mechanisms to nanostructuring. Among the most relevant ones we can find those based on metallic electrodes [13–16], interacting substrates [17–20], strain [21–23] and ferromagnetic gates [24–31]. All these mechanisms modify the fundamental properties of graphene. For instance, if we have graphene on an interacting substrate such as SiC or hBN the dispersion relation is modified and most importantly a bandgap is induced. The interaction of the graphene sheet with the substrate breaks the intrinsic sublattices symmetry in graphene and consequently a bandgap opening arises. In addition, as a result of the symmetry breaking the pseudo-spin is not longer conserved as well as Klein tunneling is prevented [32,33]. In the case of metallic and ferromagnetic gates the associated electric

* Corresponding author.
E-mail address: isaac@fisica.uaz.edu.mx (I. Rodríguez-Vargas).

https://doi.org/10.1016/j.physe.2018.03.007
Received 13 November 2017; Received in revised form 31 January 2018; Accepted 7 March 2018
Available online 7 March 2018

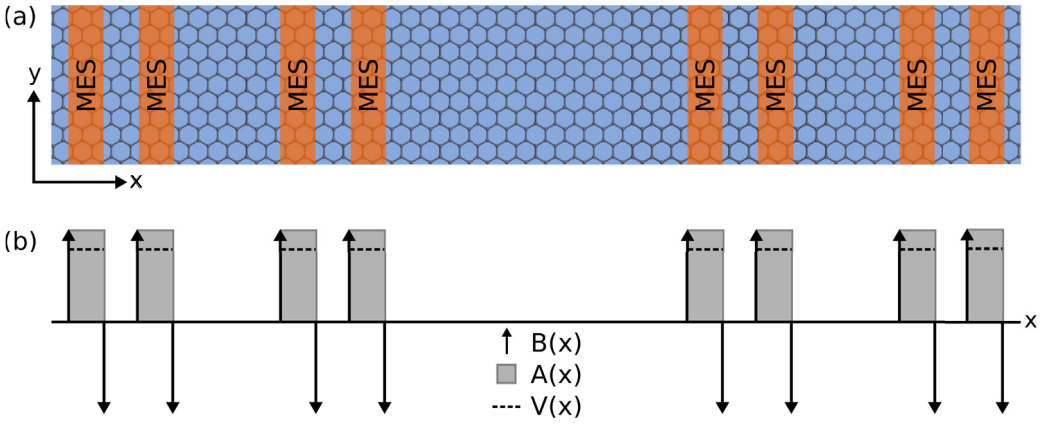

Fig. 1. (a) Schematic representation of the top view of a Cantor-like graphene-based structure under magnetoelectric effects. Graphene is placed on a non-interacting substrate like SiO_2 (shaded blue area). The magnetoelectric strips (MESs) are incorporated on top of graphene to tune the distribution and shape of the magnetic and electric fields applied perpendicularly to graphene and consequently the profile of magnetoelectric barriers. (b) Corresponding vector and scalar potential profiles for (a). The deltaic magnetic field is depicted as up and down arrows. (For interpretation of the references to colour in this figure legend, the reader is referred to the Web version of this article.)

and magnetic fields shift the graphene's Dirac cones in the energy and wavevector axis, respectively. In the case of the magnetic field, it also breaks a fundamental symmetry, specifically the time-reversal symmetry.

Under this context, the relativistic character of the charge carriers in graphene, the exotic properties that can arise due to the breaking of symmetries and the special geometries that can be imposed to graphene and other 2D materials by nanostructuration can confabulate to give place to unprecedented transmission and transport properties. In fact, in recent years, self-similar transmission and transport in graphene Cantor-like structures have been reported [34–37]. The self-similar transmittance and conductance patterns found obey well-defined scaling rules, that is, the patterns for different sizes of the system can be connected. The size of the system in the energy and spatial coordinates can be controlled by the generation and effective width of the system as well as the height of the barriers. Actually, the scaling rules correspond to precisely those parameters. Other important aspect to remark is that in order to obtain the mentioned self-similar patterns it is fundamental that the sublattices symmetry be broken, which correspond to structures with interacting substrates. Because as far as we have corroborated the self-similar characteristics are not present in structures in which the sublattices symmetry is preserved [35], i.e. structures in which the energy barriers are generated with metallic electrodes.

In this work, we study the transmission properties of graphene Cantor-like structures. In concrete, we explore the consequences of breaking the time-reversal symmetry. In order to induce the time-reversal symmetry breaking and at the same time obtain a self-similar (Cantor-like) structure we have considered that the energy barriers that composed the structure are generated by magnetic and electric fields. The magnetic field assures us the breaking of the time-reversal symmetry. The Dirac-like equation and the transfer matrix approach are implemented to describe the charge carriers and to obtain the transmission properties, respectively. We obtain that once the magnetic field is incorporated the transmission patterns show self-similar characteristics. Even more important, we obtain scaling rules that can describe the self-similar transmission patterns at different scales. To our knowledge this is the first time that scaling rules are reported under magnetic field effects.

2. Methodology

Our Cantor-like structure is composed of a graphene sheet placed on a non-interacting substrate like SiO_2. Magnetoelectric strips are considered as top gates in order to generate the magnetic and electrostatic (magnetoelectric) potential barriers along the structure, see Fig. 1. In fact, ferromagnetic strips were successfully deposited on semiconductors heterostructures [38] and constitute one of the main proposals to obtain magnetic barriers in graphene [28]. So, in principle, the strips allow us to induce different profiles for the magnetoelectric barriers. In our specific case we are considering step-wise scalar and vector potential barriers, Fig. 1 (b). These barriers are arranged according to the construction rules of the Cantor set in order to obtain our self-similar structure. A schematic representation (top view) of our Cantor-like structure is shown in Fig. 1 (a). The blue region and the orange stripes represent the SiO_2 substrate beneath the graphene sheet and the top magnetoelectric gates, respectively. Under these conditions we are dealing with two different regions corresponding to those without and with magnetoelectric barriers. The physics in these regions can be described by the corresponding Dirac-like equation. In fact, the Hamiltonian that corresponds to regions with magnetoelectric barriers is given by:

$$H = v_F \boldsymbol{\sigma} \cdot (\mathbf{p} + e\mathbf{A}) + V(x)\sigma_0, \tag{1}$$

where $\boldsymbol{\sigma} = (\sigma_x, \sigma_y)$ are the Pauli matrices, $\boldsymbol{p} = (p_x, p_y) = i\hbar\nabla$ is the momentum operator, v_F is the Fermi velocity of the Dirac electrons in graphene, $\mathbf{A} = (0, A_y, 0)$ is the vector potential given in the Landau gauge, $V(x)$ is the scalar potential and σ_0 is the 2×2 unitary matrix.

For this particular problem, we have introduced the dimensionless quantities, $l_B = \sqrt{\hbar/eB_0}$ and $E_0 = \hbar v_F / l_B$ that refer to the strength and length of the magnetic field as well as the unit of energy, respectively. Here, B_0 is a magnetic field of reference that help us to define the basic units of energy and length. In all our numerical calculations a typical realistic value of $B_0 = 0.1$ T is used, with $l_B = 811$ Å and $E_0 = 7.0$ meV [39]. Then, $\mathbf{A}(x) = A_y\hat{y} = B(B_0)l_B\hat{y}$ and $V(x) = U_0$ are defined as the vector and scalar potentials. The magnetic field B comes in terms of B_0. By solving the Dirac-like equation that corresponds to Eq. (1) it is possible to obtain the following dispersion relation:

$$E = U_0 \pm \sqrt{\hbar^2 v_F^2 q_x^2 + v_F^2(\hbar q_y + eA_y)^2}, \tag{2}$$

the $\pm$ signs correspond to electrons and holes, respectively. Moreover, the wavefunctions take the form:

$$\psi_\pm(x,y) = \frac{1}{\sqrt{2}} \begin{pmatrix} 1 \\ v_\pm \end{pmatrix} e^{\pm i q_x x + i q_y y}, \tag{3}$$

with

$$v_\pm = \frac{\hbar v_F \left(\pm q_x + i\left(q_y + \frac{e}{\hbar} A_y \right) \right)}{E - U_0}. \tag{4}$$

In addition, the wave vector in the propagation direction comes as:

$$q_x = \frac{1}{\hbar v_F} \sqrt{(E - U_0)^2 - v_F^2(\hbar q_y + eA_y)^2}. \tag{5}$$

In contrast, for regions without magnetic field the Hamiltonian come as:

$$H = v_F(\boldsymbol{\sigma} \cdot \mathbf{p}), \tag{6}$$

with a linear dispersion relation:

$$E = \pm\hbar v_F \sqrt{k_x^2 + k_y^2}, \tag{7}$$

and wavefunctions

$$\psi_{\pm}(x,y) = \frac{1}{\sqrt{2}} \begin{pmatrix} 1 \\ u_{\pm} \end{pmatrix} e^{\pm i k_x x + i k_y y}, \tag{8}$$

with

$$u_{\pm} = \frac{\hbar v_F \left(\pm k_x + i k_y\right)}{E}. \tag{9}$$

Here, the two-dimensional wave vector k is determined by Eq. (7).

With all this information, we can treat the scattering problem by means of the transfer matrix method [40,41], since we already have two different well characterised regions by its appropriate energy dispersion relation, wave vector and wavefunction. Considering the continuity condition of the wavefunction in each boundary of the structure along the propagation direction (x direction) as well as the conservation of the momentum in the transversal direction ($k_y = q_y$), we can find a matrix connection between the amplitudes of the incoming waves in terms of the outgoing waves via the expression:

$$\begin{pmatrix} A_0 \\ B_0 \end{pmatrix} = \begin{pmatrix} M_{11} & M_{12} \\ M_{21} & M_{22} \end{pmatrix} \begin{pmatrix} A_{N+1} \\ 0 \end{pmatrix}, \tag{10}$$

where the transfer matrix M is given as:

$$M = D_0^{-1} \left[\prod_{j=1}^{N} D_j P_j D_j^{-1} \right] D_0, \tag{11}$$

with D_j as the dynamical matrices which take the form:

$$D_j = \begin{cases} \begin{pmatrix} 1 & 1 \\ u_+ & u_- \end{pmatrix}, \\ \\ \begin{pmatrix} 1 & 1 \\ v_+ & v_- \end{pmatrix}, \end{cases} \tag{12}$$

and P_j the propagation matrices written explicitly as:

$$P_j = \begin{cases} \begin{pmatrix} e^{-ik_x(x_{j+1}-x_j)} & 0 \\ 0 & e^{ik_x(x_{j+1}-x_j)} \end{pmatrix}, \\ \\ \begin{pmatrix} e^{-iq_x(x_{j+1}-x_j)} & 0 \\ 0 & e^{iq_x(x_{j+1}-x_j)} \end{pmatrix}, \end{cases} \tag{13}$$

where k_x (q_x) is the x component of the wave vector k (q) for regions without (with) magnetic field and $x_{j+1} - x_j$ is the width of the j-th region with $j = 0,1,2,\ldots,$ N.

Thus, the transmittance or transmission coefficient can be computed as:

$$T = \frac{1}{|M_{11}|^2}. \tag{14}$$

3. Results

With the previous formalism at hand, we are in possibility to deal with our central goal which is to explore scaling relations for the self-similar transmission patterns. In particular, we look for scaling rules as function of two principal parameter: the generation N and the length of the system w.

First, we start by comparing the transmission curves between two consecutive generations. This with the aim to find out if in reality self-similarity between generations exists. To this respect, Fig. 2 (a) shows the transmittance as function of the energy for Dirac electrons at oblique incidence ($\theta = \pi/4$). Here the solid-black and the dashed-red lines correspond to generations $N = 7$ and $N = 8$, respectively. The rest of the structural parameters are fixed such as the magnetic field strength $B = 2B_0$, electric field intensity $U_0 = 2E_0$ and length of the system $w = 20\, l_B$. From the figure we can see that the transmission curves are perfectly correlated and only differ in their amplitudes. Hence, it is likely that the scaling transformation be a certain power of the transmittance. Specifically, we propose

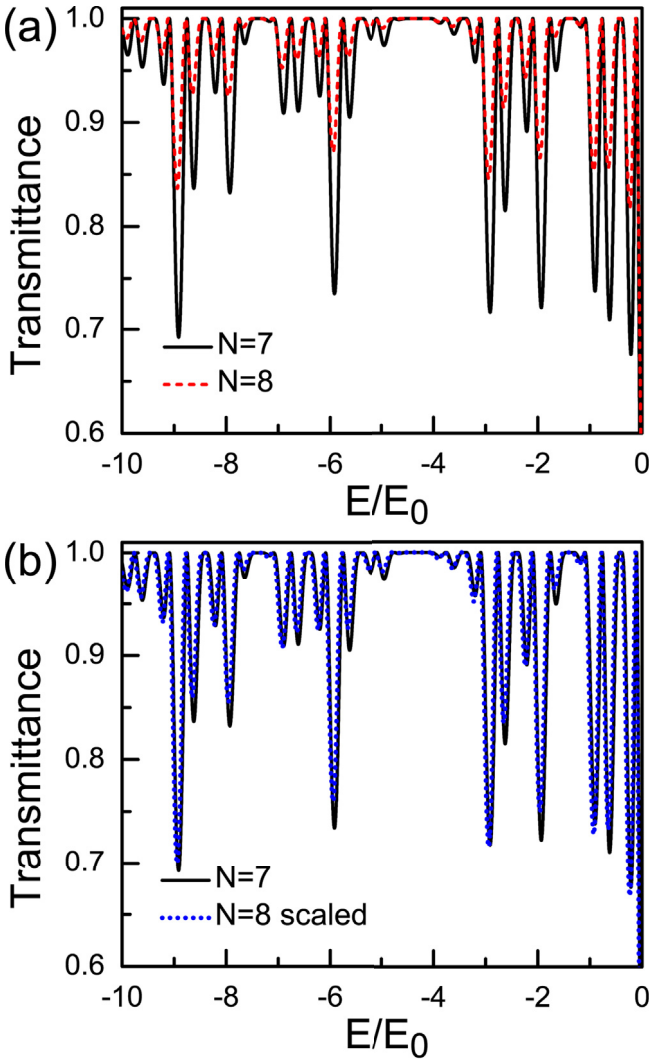

Fig. 2. Scaling between generations. (a) Transmittance as function of the energy for generations $N = 7$ (solid-black lines) and $N = 8$ (dashed-red lines). (b) The same as in (a) but here the generation $N = 8$ (dotted-blue lines) is scaled in accordance with Eq. (15). In this case the scaled curve resembles quite good to the reference one ($N = 7$). The structural parameters are $B = 2B_0$, $U_0 = 2E_0$ and $w = 20\, l_B$. (For interpretation of the references to colour in this figure legend, the reader is referred to the Web version of this article.)

$$T_N(E) \approx [T_{N+1}(E)]^2. \tag{15}$$

Then, to prove this expression we simply denote T_7 and T_8 as the reference and scaled curves, respectively. Thus, Eq. (15) takes the form $T_7(E) \approx [T_8(E)]^2$. The resulting scaling is shown in Fig. 2 (b), we can notice that the scaled curve (dotted-blue lines) has an excellent matching with respect to the reference one (solid-black lines). Then turns out that our proposed expression effectively describes the scaling between generations.

In the case of the length of the system, we found that when one treats two structures with different lengths, the transmittance patterns have self-similar features, see Fig. 3 (a). In this case, we have consid-

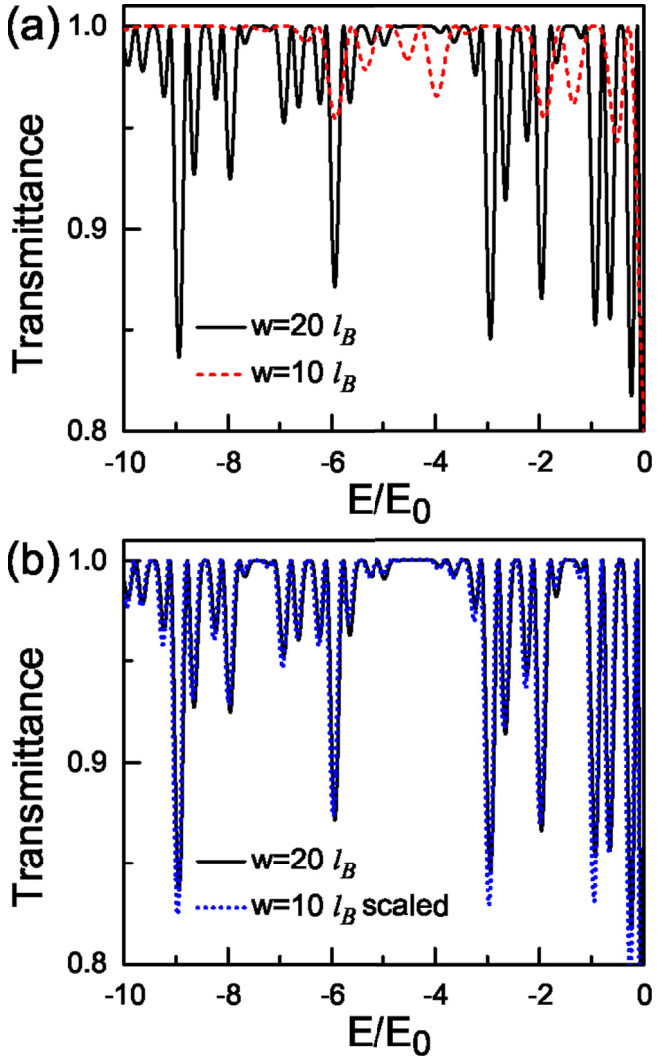

Fig. 3. Scaling between lengths. (a) Transmittance as function of the energy for lengths $w = 20\, l_B$ (solid-black lines) and $w = 10\, l_B$ (dashed-red lines). (b) The same as in (a) but here the length $w = 10\, l_B$ (dotted-blue lines) is scaled in accordance with Eq. (16). The scaled curve is very similar to the reference one ($w = 10\, l_B$). The structural parameters are $N = 8$, $B = 2B_0$ and $U_0 = 2E_0$. (For interpretation of the references to colour in this figure legend, the reader is referred to the Web version of this article.)

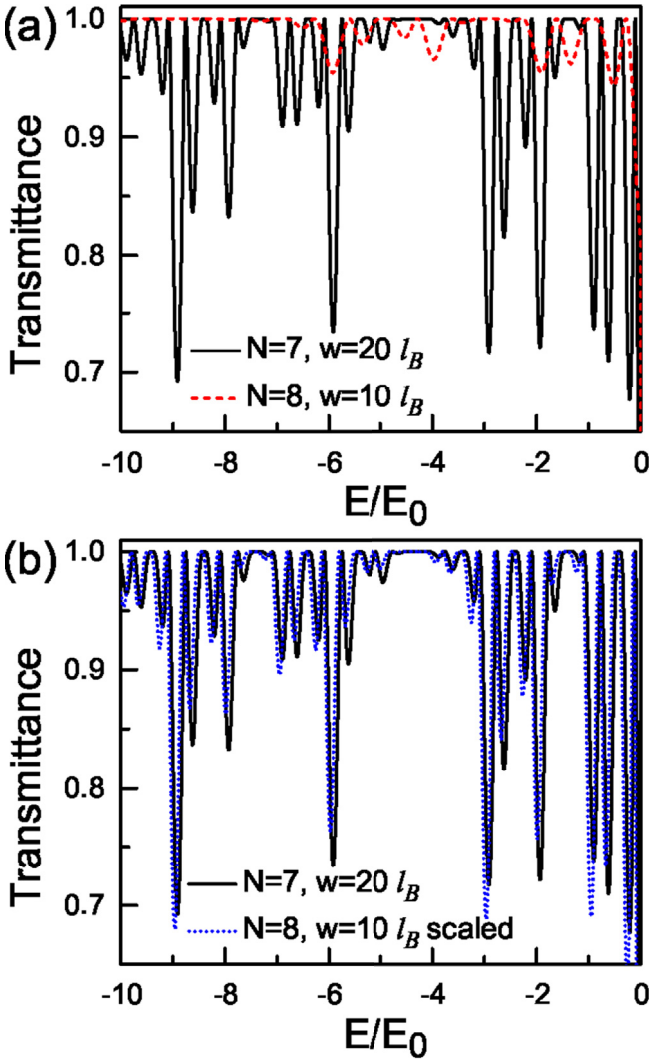

Fig. 4. General scaling. (a) Transmittance as function of the energy for $N = 7$ and $w = 20\, l_B$ (solid-black lines) and $N = 8$ and $w = 10\, l_B$ (dashed-red lines). (b) The same as in (a) but here the scaled curve (dotted-blue lines) is computed in accordance with Eq. (17). The scaled curve is very similar to the reference one (solid-black lines). The structural parameters are $B = 2B_0$, $U_0 = 2E_0$ and $\theta = \pi/4$. (For interpretation of the references to colour in this figure legend, the reader is referred to the Web version of this article.)

ered two lengths $w = 20\, l_B$ and $w = 10\, l_B$, solid-black lines and dashed-red lines, respectively. The rest of the parameters are the same as in Fig. 2, except that here the generation $N = 8$ remains fixed. Alike to the generation case, we need to apply some transformation in order to be able to reproduce the reference curve by means of the scaled one. The corresponding transformation that we are proposing is

$$T_w(E) \approx [T_{\frac{1}{\alpha}w}(\frac{1}{\alpha}E)]^{\alpha^2}, \tag{16}$$

where w indicates the length of the system and α is the factor that connects the lengths of both structures: the reference structure and the scaled one.

By applying Eq. (16) to our particular results, we obtain the expression $T_{20_{l_B}}(E) \approx [T_{10_{l_B}}(\frac{1}{2}E)]^4$. As we can notice, two transformations are needed for this scaling. The first one modifies the transmittance axis by rising it to the fourth power, while the second one implies to reduce by a factor 2 the energy axis. The result of these transformations is shown in Fig. 3 (b). The dotted-blue lines correspond to the scaled curve, while the solid-black lines represent the reference curve. Comparing both transmission curves we can appreciate that these curves match quite well.

The preceding scaling expressions, Eq. (15) and Eq. (16), can also be combined to give us a general scaling rule,

$$T(E, N, w) \approx [T(\frac{1}{\alpha}E, N + m, \frac{1}{\alpha}w)]^{2^{m(\alpha)^2}}, \tag{17}$$

where m is the difference between generations and α is the value that connects the ratio between the lengths of the systems. According to this general scaling we can compare two transmission curves with non-consecutive generations and different lengths. Despite the two parameters involved in the general rule as well as non-consecutive generations it is possible to obtain very good scaling between the transmission patterns, see Fig. 4.

In order to have a quantitative analysis between the self-similar transmission curves a study of the root mean square deviation (rmsd) is considered. rmsd gives us a numerical value that indicates quantitatively how similar are the scaled and reference curves. If the rmsd tends to zero it means that the matching between the curves is quite good. For the scaling between generations and lengths the rmsd values are 2.95089167E-02 and 1.90727431E-02, respectively. Thus, as we can see the best scaling takes place between lengths of the system.

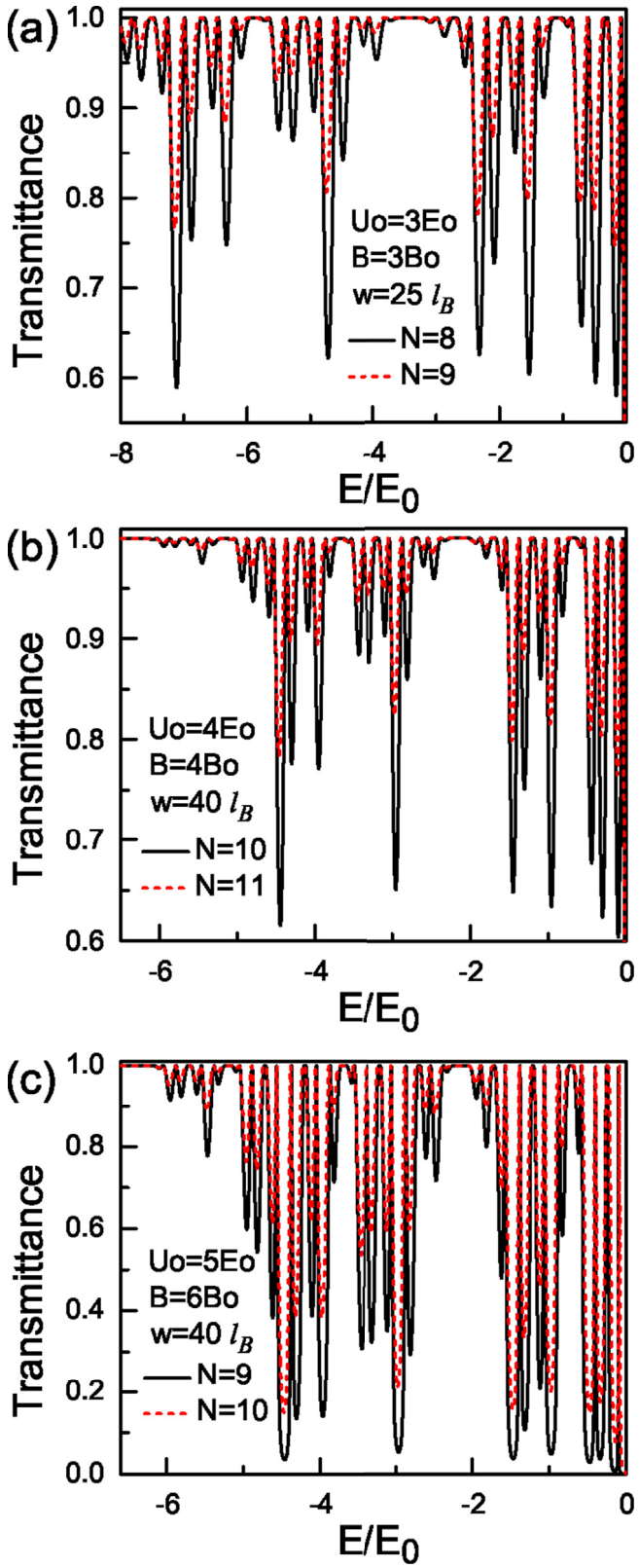

Fig. 5. Transmission patterns for different heights of the electrostatic barriers: (a) $U_0 = 3E_0$, (b) $U_0 = 4E_0$, and (c) $U_0 = 5E_0$. In order to have self-similar transmission patterns the length of the system and the magnetic field strength need to be adjusted. In fact, in (a) $w = 25\, l_B$ and $B = 3B_0$, while in (b) $w = 40\, l_B$ and $B = 4B_0$, and in (c) $w = 40\, l_B$ and $B = 6B_0$. Likewise, the generations of the self-similar structure need to be adjusted as well, see the difference between (a), (b) and (c). The angle of incidence in all cases is the same, $\theta = \pi/4$.

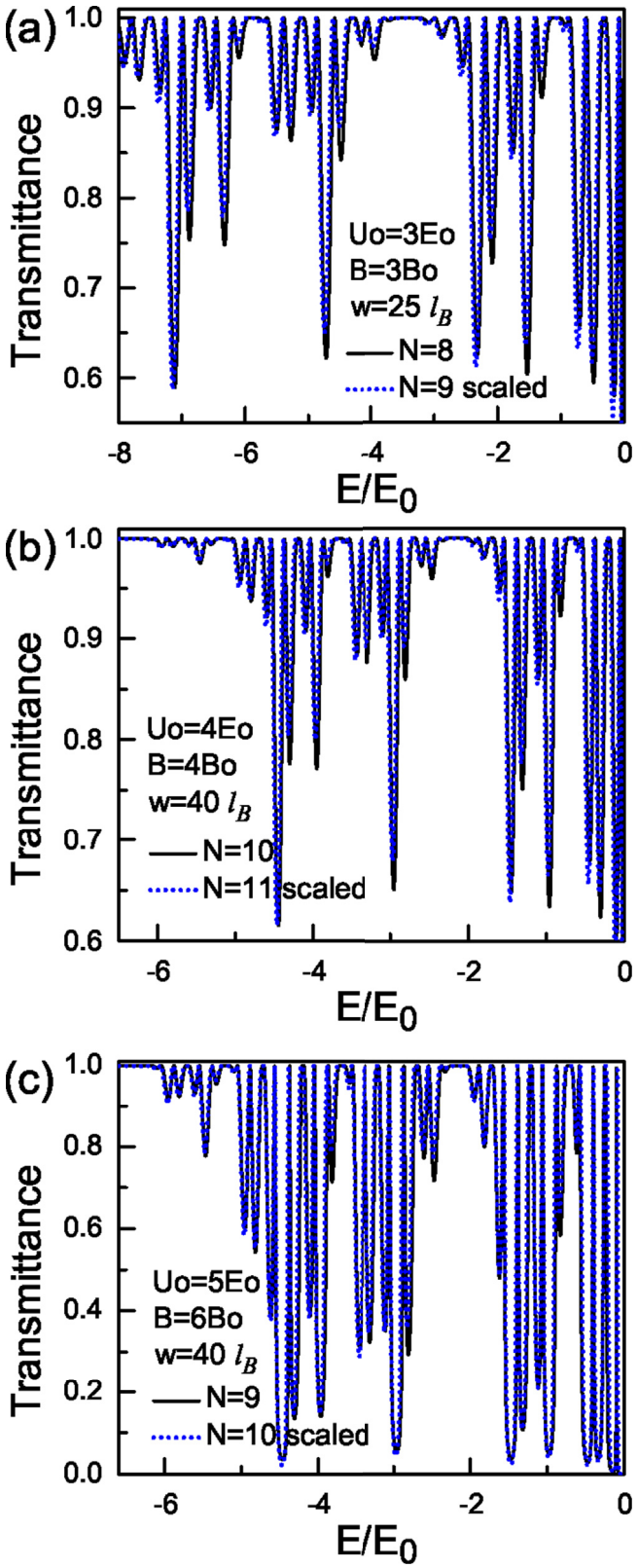

Fig. 6. The same as in Fig. 5, but here the scaling between generations, Eq. (15), has been applied. As we can see this rule is well obeyed regardless of the height of the electrostatic barrier.

4. Discussion

In this section, we want to discuss three aspects that we consider relevant to have a better understanding of the self-similar transmission patterns.

The first one is related to the fact that the scaling is only presented for holes, see the energy axis in all figures. In graphene-based structures it is well known that electrons and holes respond in different ways to magnetic fields. However, we do not have a definite answer about why only the hole spectrum manifests self-similar patterns. Even more interesting, if the polarity of the magnetic field is inverted, the self-similar patterns will arise in the electron spectrum.

The second aspect that is important to comment is about the magnetic field strength at which the self-similar patterns are taking place. In fact, for all our results the critical magnetic field takes a value of $2B_0$. This seems to be a special value for our structure. However, for larger magnetic fields the transmission patterns are shifted in both the transmittance and energy axis, maintaining the envelope of the curves. So, it is possible that other scaling rules, in which the magnetic field strength be involved, describe these transmission patterns. Furthermore, if we change the height of the electrostatic barriers it is necessary to adjust the length of the system as well as to modify the magnetic field strength in order to have self-similar transmission patterns. In Fig. 5 we show the corresponding results for: (a) $U_0 = 3E_0$, (b) $U_0 = 4E_0$ and (c) $U_0 = 5E_0$. In the first case $U_0 = 3E_0$, we need to adjust w and B to 25 l_B and $3B_0$, respectively; while for $U_0 = 4E_0$ these parameters need to adopt the values $w = 40\ l_B$ and $B = 4B_0$; and for the third case $U_0 = 5E_0$, the length of the system and the magnetic field strength required are $w = 40\ l_B$ and $B = 6B_0$, respectively. Here, it is also important to mention that the generations of the self-similar structure need to be adjusted as well. In fact, for (a), (b) and (c) the self-similar transmission patterns are presented for $N = 8$ and $N = 9$, $N = 10$ and $N = 11$, and $N = 9$ and $N = 10$, respectively. This is a quite relevant because the interplay between these parameters will determine the characteristics of the transmission patterns. From the experimental standpoint it is also preponderant because we need to choose accessible values for the electrostatic field intensity, the magnetic field strength and the length of the system that guarantee self-similar transmission patterns. Likewise, it is important to remark that the scaling rule between generations remains the same regardless of the height of the electrostatic barriers, see Fig. 6.

The third and last aspect that we want to address is the one related to resonant states. In fact, the well regions in our structure serve as resonant cavities. For instance, the second generation $N = 2$ of our system has a well with a width $w/3$, while in the case of $N = 3$ in addition to the well region $w/3$ there is another well with a width $w/9$. Then, every time that we increase the generation we add an extra well region that is a third of the last added in the previous generation. With this in mind, the condition for resonant states in one of these regions can be written as,

$$k_x w/3^{N-1} = n\pi, \tag{18}$$

where n is an integer. From this condition the energy of the resonant states is given as

$$E_n(N) = \frac{3^{N-1}\sec\theta}{w} n\pi, \tag{19}$$

or equivalently in terms of the resonant states of $N = 2$,

$$E_n(N) = 3^{N-2} E_n(2). \tag{20}$$

Here, $E_n(N)$ and w are given in units of E_0 and l_B, respectively.

Then, for example, $E_n(3)$ and $E_n(2)$ determine the resonant states for the third generation. For the fourth generation $E_n(4)$, $E_n(3)$ and $E_n(2)$ provide the resonant state energies. For the specific case presented in Fig. 2, the difference between generation 7 and 8 is $E_n(8)$. However, from the resonant states standpoint these generations are the same, because the resonant states provided by $E_n(8)$ lie outside the energy region considered. Actually, above generation 4 we do not have differences in the resonant states that come from the well regions. In fact, the first resonant level of $E_n(5)$ lies outside the energy range, $E_1(5) \approx 18E_0$.

A similar analysis can be done for the barriers. However, in this case all barriers, for a given generation, have the same size. Another important aspect and a substantial difference with respect to Schrödinger electrons is that barriers can support resonant states, even for energies below the barrier height.

As in the case of well regions the condition for resonant states in the barriers comes as

$$q_x w/3^{N-1} = m\pi, \tag{21}$$

with m an integer. By replacing q_x and solving for the energy we obtain,

$$|E_m(N)| = \frac{(U_0 - B\sin\theta)}{\cos^2\theta} \times \left[-1 + \sqrt{1 + \frac{\cos^2\theta}{(U_0 - B\sin\theta)^2}\left(\frac{m^2\pi^2}{w^2}3^{2(N-1)} + B^2 - U_0^2\right)}\right]. \tag{22}$$

Here, U_0 and B are dimensionless quantities given in units of E_0 and B_0, respectively. It is also important to mention that this expression is valid for holes. For the specific case of $U_0 = B$, Eq. (22) can be simplified to

$$|E_m(N)| = U_\theta\left[-1 + \sqrt{1 + \frac{1}{U_\theta^2\cos^2\theta}\frac{m^2\pi^2}{w^2}3^{2(N-1)}}\right], \tag{23}$$

where $U_\theta = U_0(1 - \sin\ \theta)/\cos^2\theta$.

For the parameters and the energy range considered in Fig. 2 we obtain 6 and 2 resonant hole states for generations 3 and 4, whereas generations 5, 6, 7 and 8 have their first resonant level outside the energy range. These characteristics are quite interesting because precisely the transmission patterns that are self-similar have practically the same resonant states. Further studies in other self-similar structures are needed in order to see if these characteristics about resonant states are preponderant and determined in some way the self-similar transmission patterns.

5. Conclusions

In summary, we have investigated the self-similar transmission properties in Cantor-like graphene-based structures. The Dirac-like equation and the transfer matrix approach were implemented to describe the charge carriers in graphene and to obtain the transmission properties, respectively. We obtained that once the magnetic field is incorporated self-similar patterns arise in the transmittance. Furthermore, these patterns obey well-defined scaling rules that account for the connection between patterns at different generations and lengths of the system. Finally, it is important to remark that the relativistic character of the charge carriers, the time-reversal symmetry breaking and the special nanostructuration of the material are confabulated to give rise to this peculiar transmission properties. Our results also support the thesis that the breaking of some symmetry is fundamental to obtain self-similar transmission and transport properties in graphene [35,37].

Acknowledgments

R.R.-G. acknowledges to CONACYT-Mexico for the scholarship for doctoral studies.

References

[1] J.E. Moore, L. Balents, Phys. Rev. B 75 (2007) 121306.
[2] L. Fu, C.L. Kane, Phys. Rev. B 76 (2007) 045302.
[3] M.Z. Hasan, C.L. Kane, Rev. Mod. Phys. 82 (2010) 3045.
[4] S.M. Young, S. Zaheer, J.C. Teo, C.L. Kane, E.J. Mele, A.M. Rappe, Phys. Rev. Lett. 108 (2012) 140405.

[5] Z.K. Liu, et al., Science 343 (2014) 864.
[6] X. Wan, A.M. Turner, A. Vishwanath, S.Y. Savrasov, Phys. Rev. B 83 (2011) 205101.
[7] A.A. Burkov, Leon balents, Phys. Rev. Lett. 107 (2011) 127205.
[8] M. Orlita, et al., Nat. Phys. 10 (2014) 233.
[9] A. Akrap, et al., Phys. Rev. Lett. 117 (2016) 136401.
[10] G.W. Semenoff, Phys. Scripta T186 (2012) 014016.
[11] L.M. Gaggero-Sager, E.R. Pujals, O. Sotolongo-Costa, Phys. Status Solidi 220 (2000) 167.
[12] L.M. Gaggero-Sager, E. Pujals, D.S. Díaz-Guerrero, J. Escorcia-García, Self-similarity in Semiconductors: Electronic and Optical Properties, Optoelectronics - Materials and Techniques, Prof. P. Predeep, InTech, 2011.
[13] J. Milton Pereira Jr., P. Vasilopoulos, F.M. Peteers, Appl. Phys. Lett. 90 (2007) 132122.
[14] X. Chen, J.-W. Tao, Appl. Phys. Lett. 94 (2009) 262102.
[15] J.M. Pereira Jr., F.M. Peteers, A. Chaves, G.A. Farias, Semicond. Sci. Technol. 25 (2010) 033002.
[16] R. Biswas, S. Mukhopadhyay, C. Sinha, Physica E 42 (2010) 1781.
[17] S.Y. Zhou, G.-H. Gweon, A.V. Fedorov, P.N. First, W.A. de Heer, D.-H. Lee, F. Guinea, A.H. Castro Neto, A. Lanzara, Nat. Mater. 6 (2007) 770.
[18] G. Giovannetti, P.A. Khomyakov, G. Brocks, P.J. Kelly, J. van den Brink, Phys. Rev. B 76 (2007) 073103.
[19] X. Peng, R. Ahuja, Nano Lett. 8 (2008) 4464.
[20] C.R. Dean, A.F. Young, I. Meric, C. Lee, L. Wang, S. Sorgenfrei, K. Watanabe, T. Taniguchi, P. Kim, K.L. Shepard, J. Hone, Nat. Nanotechnol. 5 (2010) 722.
[21] G. Gui, J. Li, J. Zhong, Phys. Rev. B 78 (2008) 075435.
[22] F. Guinea, M.I. Katsnelson, A.K. Geim, Nat. Phys. 6 (2010) 30.
[23] F.M.D. Pellegrino, G.G.N. Angilella, R. Pucci, Phys. Rev. B 84 (2011) 195404.
[24] A. De Martino, L. Dell'Anna, R. Egger, Phys. Rev. Lett. 98 (2007) 066802.
[25] A. De Martino, L. Dell'Anna, R. Egger, Solid State Commun. 144 (2007) 547.
[26] M. Ramezani Masir, P. Vasilopoulos, F.M. Peeters, Appl. Phys. Lett. 93 (2008) 242103.
[27] M. Ramezani Masir, P. Vasilopoulos, A. Matulis, F.M. Peeters, Phys. Rev. B 77 (2008) 235443.
[28] M. Ramezani Masir, P. Vasilopoulos, F.M. Peeters, N. J. Phys. 11 (2009) 095009.
[29] S. Ghosh, M. Sharma, J. Phys. Condens. Matter 21 (2009) 292204.
[30] L. Dell'Anna, A. De Martino, Phys. Rev. B 79 (2009) 045420.
[31] L. Dell'Anna, A. De Martino, Phys. Rev. B 83 (2011) 155449.
[32] M.I. Katsnelson, K.S. Novoselov, A.K. Geim, Nat. Phys. 2 (2006) 620.
[33] P.E. Allain, J.N. Fuchs, Eur. Phys. J. B 83 (2011) 301.
[34] D.S. Díaz-Guerrero, L.M. Gaggero-Sager, I. Rodríguez-Vargas, O. Sotolongo-Costa, Europhys. Lett. 111 (2015) 57006.
[35] R. Rodríguez-González, I. Rodríguez-Vargas, D.S. Díaz-Guerrero, L.M. Gaggero-Sager, Eur. Phys. J. B 89 (2016) 17.
[36] D.S. Díaz-Guerrero, I. Rodríguez-Vargas, G.G. Naumis, L.M. Gaggero-Sager, Fractals 24 (2016) 1630002.
[37] H. García-Cervantes, L.M. Gaggero-Sager, D.S. Díaz-Guerrero, O. Sotolongo-Costa, I. Rodríguez-Vargas, Sci. Rep. 7 (2017) 617.
[38] A. Nogaret, D.N. Lawton, D.K. Maude, J.C. Portal, M. Henini, Phys. Rev. B 67 (2003) 165317.
[39] F. Zhai, K. Chang, Phys. Rev. B 77 (2008) 113409.
[40] P. Yeh, Optical Waves in Layered Media, Wiley-Interscience, 2005.
[41] P. Markos, C.M. Soukoulis, Wave Propagation: from Electrons to Photonic Crystals and Left-handed Materials, Princeton University Press, 2008.